Local Voltage Drop in a Single Functionalized Graphene Sheet Characterized by Kelvin Probe Force Microscopy

Liang Yan,[†,§] Christian Punckt,[‡,§] Ilhan A. Aksay,[‡] Wolfgang Mertin,[*,†] and Gerd Bacher[†]

[†]Werkstoffe der Elektrotechnik and CeNIDE, Universität Duisburg-Essen, 47057 Duisburg, Germany

[‡]Department of Chemical and Biological Engineering, Princeton University, Princeton, New Jersey 08540, United States

ABSTRACT: We studied the local voltage drop in functionalized graphene sheets of sub μm size under external bias conditions by Kelvin probe force microscopy. Using this noninvasive experimental approach, we measured ohmic current–voltage characteristics and an intrinsic conductivity of about 3.7×10^5 S/m corresponding to a sheet resistance of 2.7 kΩ/sq under ambient conditions for graphene produced via thermal reduction of graphite oxide. The contact resistivity between functionalized graphene and metal electrode was found to be $<6.3 \times 10^{-7}$ Ωcm^2.

KEYWORDS: Functionalized graphene, Kelvin probe force microscopy, electrical conductivity, contact resistance, sheet resistance
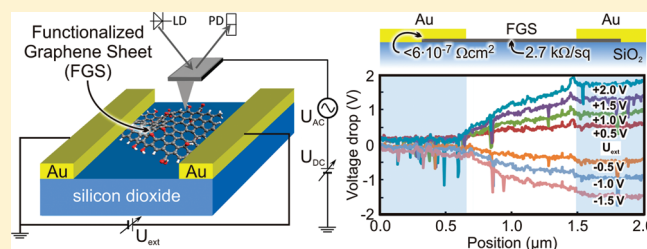
While various efforts have focused on the isolation of reduced graphene oxide through exfoliation of graphite oxide (GO) for more than 150 years,[1−8] more recent measurements performed on pristine, mechanically exfoliated graphene by Novoselov et al.[9] suddenly generated immense interest in graphene due to its unique electronic,[9−11] mechanical,[12,13] and thermal[14,15] properties. In particular its superior electronic properties, e.g., electron mobility of 10^4 cm^2 V^{-1} s^{-1} at a charge carrier density of 10^{12} cm^{-2} on a SiO$_2$ substrate at room temperature,[16] made graphene a promising candidate for replacing semiconductors in future electronic devices.[17,18] Mechanically exfoliated, pristine graphene is still the material of choice for proof-of-concept microelectronic device research[16] and fundamental studies,[19] but graphene grown epitaxially on SiC[20,21] or other substrates[22,23] is probably most suitable for the development of practical microelectronic devices. For the development of bulk materials such as graphene-based ultracapacitors,[24] electrodes for batteries,[25−27] electrochemical sensors,[28−30] and graphene-based composites in general,[31,32] however, there is a need to produce graphene in bulk powder form.

For applications where graphene is needed in bulk quantities, the GO-based route to graphene has proven to be the most suitable method so far.[6−8,33] Thus, while the GO preparation has only been slightly modified since the 19th century,[3,34] its exfoliation into single sheet graphene oxide, first demonstrated by Wen et al.,[35] and its reduction to lower oxygen contents have received great interest in recent years.[33] The reduction of graphene oxide can be performed either by solution chemistry approaches[4,8] or by thermal exfoliation of GO.[6,7] The latter process has already been adopted for the production of graphene powder in tons per year quantities.[36] Graphene produced by thermal exfoliation and reduction of GO exhibits a specific surface area of 700−1850 m^2/g and contains a large fraction of single sheets[6,7] decorated with oxygen-containing functional groups and exhibiting lattice defects (Figure 1a).[37−40] We refer to this material as functionalized graphene sheets (FGSs).

FGSs have been used in various applications: In lithium ion batteries they improved the electrical conductivity of electrode materials leading to near theoretical power density.[25−27] Supercapacitor applications benefited from the large surface area and the apparently good electrical conductivity of FGSs resulting in large specific capacity and power density.[24] Functional groups and lattice defects have been shown to contribute to electrocatalytic properties of FGSs,[28−30,41] and in electrically conducting polymer nanocomposites, FGSs lead to improved mechanical and thermal properties.[31,32]

In particular for applications in polymer nanocomposites and electrical energy storage devices, both the intrinsic FGS resistance and the contact resistance between adjacent sheets or between a sheet and the (often metallic) electrode are important factors controlling the device performance. Macroscopic characterization techniques such as four-point probe methods or transfer length measurements are state of the art for extracting electronic conductivity[16,21,42] and contact resistance[43,44] of single functionalized or pristine graphene sheets. However, these macroscopic techniques only allow spatially averaged measurements while the impact of microscopic features of laterally inhomogeneous materials, such as defective graphene, or the potential drop at graphene–metal contacts remains hidden. Spatially resolved microscopic techniques such as scanning tunneling microscopy (STM),[45−47] Kelvin probe force microscopy (KPFM), and electrostatic force microscopy (EFM)[48−50] overcome these limitations and give insight into local electrical properties of any studied graphene. STM has been used to study impurity-induced charge density fluctuations in pristine graphene,[45] as well as the influence of wrinkles on the conductivity of mechanically exfoliated graphene[46] and
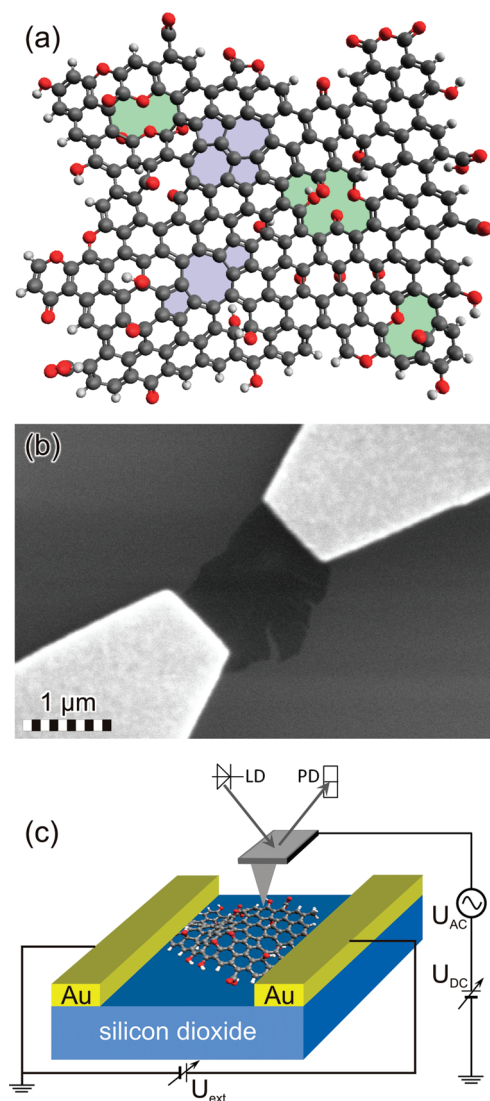
Figure 1. (a) Schematic of a FGS showing various functional groups decorating the edge of the sheet (such as anhydrides, carboxylic acid, and ethers), lattice defects (5−8−5 defect (double vacancy) and 5−7−7−5 (Stone−Wales) defect, light blue), oxygen decorated vacancies (light green), as well as epoxy and hydroxyl groups on both sides of the graphene plane. Carbon atoms are gray, oxygen atoms are red, and hydrogen atoms are white. (b) SEM image of an FGS on a silicon dioxide substrate contacted with two gold pads. (c) Schematic of the KPFM setup indicating the applied dc and ac voltages.

epitaxial layers of graphene,[47] i.e., structures which are not FGS-type. KPFM and EFM have, for example, been used recently to study the impact of graphene layer thickness on the work function and the surface potential of mechanically exfoliated graphene with varying back gate voltage.[51−53] The local work function of epitaxially grown graphene on SiC was also studied by KPFM,[54] and the contact resistance between mechanically exfoliated graphene and Au/Cr contacts was derived by surface potential mapping using KPFM.[53] Such techniques are particularly useful to study the local properties of individual FGSs because the large density of functional groups and lattice defects of FGSs is expected to strongly influence their electrical properties and to affect the performance of FGS-based devices.

Until now, however, measurements of the intrinsic conductivity of individual chemically or thermally reduced graphene oxide sheets (prepared in a different way than the FGSs used here) have only been performed using classical four- or simple two-point techniques,[42,55,56] and the values of the corresponding sheet resistances are on the order of several MΩ/sq. These values are 3 orders of magnitude above the intrinsic maximum resistivity of pristine (i.e., mechanically exfoliated) graphene of 6.45 kΩ/sq.[16,57−60] This is likely due to the large amount of oxygen-containing functional groups and defects of reduced graphene oxide leading to decreased charge carrier mobility[52] and is analogous to observations with artificially defected pristine graphene.[55,61]

FGSs produced by the thermal reduction of GO used in our work exhibit both a large number density of functional groups (similar to chemically reduced graphene oxide) and lattice defects.[6] Therefore, their intrinsic electrical conductivity is expected to be dominated by defect scattering (possibly resulting in a resistivity on the order of MΩ/sq). On the other hand, a recent study by Jafri et al. suggests that acid treatment of carbon nanosheets (which creates vacancy defects) leads to a conductivity increase compared to the untreated carbon sheets which is caused by an increase of the charge carrier density and results in a material with a sheet resistance of only 3.5 kΩ/sq.[62] Therefore, our material may exhibit a comparably large charge carrier density leading to a large conductivity despite reduced mobility.

Here, we present KPFM measurements of individual FGSs under ambient conditions with the goal to determine their intrinsic conductivity, the nature of the charge transport between FGS and metal contacts, as well as potential correlations between electrical properties and topographic or structural features. Our results indicate that FGSs derived through thermal exfoliation of GO have a surprisingly large electrical conductivity of up to 3.7×10^5 S/m (sheet resistance 2.7 kΩ/sq). Charge transfer between metal contacts and FGSs is fully symmetric, and no significant potential drop is observed between the metal and FGS (noninvasive contact) suggesting that the functional groups and defects might facilitate charge transfer. This observation agrees with recent measurements on chemically derived reduced functionalized graphene[56] (exhibiting resistances of several megaohms) and is contrary to what has been observed for mechanically exfoliated graphene where the contacts perturb the electronic structure of graphene and lead to large contact resistances.[53]

In the context of electrical energy storage and polymer nanocomposites, our results indicate that FGSs are well suited as additives for such applications because they exhibit a comparably large intrinsic conductivity. Furthermore, the observation of noninvasive FGS−gold contacts suggests that the presence of functional groups and defects in our material might facilitate charge transport in systems using FGS as conductive filler.

Experimental Details. The process to derive FGSs is described in detail elsewhere.[6,7] FGSs suspended in ethanol (at a concentration <0.1 mg/mL) were deposited on a 300 nm thick SiO_2 layer grown on a Si substrate. After evaporation of the solvent (overnight) the position of individual sheets was measured optically with respect to predefined alignment marks, and electron beam lithography was used to fabricate two contacts for each FGS, consisting of a 10 nm thick Ti adhesion layer and 100 nm thick layer of gold. Figure 1b shows a scanning electron microscopy (SEM) image of an individual contacted FGS.

For the KPFM measurements, we utilized a home-built Kelvin controller integrated into a Veeco diInnova atomic force microscopy (AFM) system, allowing topography and Kelvin voltage to be measured simultaneously with a spatial resolution of about 20 nm and a potential resolution of a few millivolts.[48,50] During scanning in the one-pass mode, the cantilever oscillates at its first and second resonance frequencies superimposed. The first resonance frequency is used as the feedback signal for measuring the topography (as in standard AFM topography imaging), while at the same time the second resonance frequency is used to determine the electrical surface potential. This one-pass method provides an improved spatial resolution for the Kelvin measurements compared to the conventional two-pass method (also called lift-mode) typically used by others,[49,53] because the tip oscillates at a much closer distance above the sample surface. This allows us to spatially resolve the impact of distinct, nanometer-sized topographic features on the local potential distribution in a contacted FGS. We used silicon KPFM probes (Budget Sensor, ElectriMulti75G) with a symmetric tip shape (nominal radius <25 nm) which were coated with a conductive Cr/PtIr layer (5 nm Cr and 25 nm PtIr) on both sides of the cantilever and had a first resonance frequency of about 75 kHz. While employing this resonance frequency for topography imaging, we simultaneously applied a modulation voltage V_{AC} of 1.0 V at a frequency of 400−435 kHz (second resonance frequency of the cantilever) for the ac signal of the Kelvin measurements. External biases V_{ext} ranging from −1.5 to +2.0 V were applied to study the local electrical potential distribution in an electrode configuration as shown in Figure 1c. During scanning, the electrical current corresponding to the external bias was recorded by a source meter. All measurements were conducted in noncontact mode under ambient conditions at ∼21 °C and relative humidity of ∼45%.

Results and Discussion. In panels a and b of Figure 2, we show topography images of a contacted FGS. A complex topography, including distinct height steps and a variety of wrinkles (one-dimensional, wormlike features), is observed on the graphene sheet. Large wrinkles can also be seen underneath the metal electrodes where the graphene sheet is in physical contact with the gold. The observed topographical features can be the result of a variety of different effects. During evaporation of the FGS suspension, an individual sheet is subjected to capillary forces as the suspension medium evaporates. As the sheet approaches the substrate during drying, van der Waals forces can lock parts of the sheet in a fixed position before the sheet can fully flatten out.[6,63] This may cause the sheet to adhere in a somewhat crumpled configuration. Parts of the sheet can also be folded onto itself:[63] In Figure 2c, an enlarged topography line scan across a small area close to the left contact is shown, indicating a height step of about 3−4 nm of the FGS. The height of the left part of the line scan is presumably caused by a stacking of several FGS layers because enlarged plateaus on both sides of the step can be recognized. The height of the right part (∼1 nm) corresponds well to previous measurements of the thickness of a single layer of functionalized graphene by AFM.[6] Note, that the enhanced thickness compared to the value expected for pristine graphene is due to the functional groups decorating the carbon backbone as well as the presence of lattice defects causing sheet deformations).[6] The production of FGSs results in functional groups and lattice defects[38] (Figure 1a) which are known to introduce bumps and folds in the carbon grid and to increase the spacing between adjacent layers compared to pristine graphene.[6,63] Therefore, the small wrinkles (<1 nm in height)
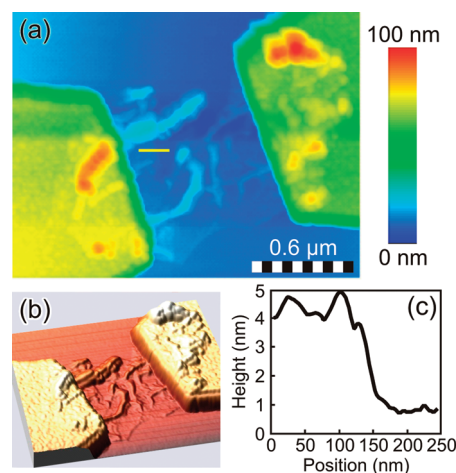

Figure 2. (a) Topography image of a contacted FGS. The uncovered part of the graphene sheet measures approximately 790 nm × 920 nm in size. (b) Three-dimensional representation of sheet topography corresponding to (a). (c) Line scan of a height step indicated by the yellow line in (a).

visible in the AFM image may be caused by clusters of epoxy and hydroxy sites and lattice defects. In the following, we measure the Kelvin voltage of a single graphene sheet with and without applied bias. The measurements are related to the observed sample topography and compared to existing data in the literature for pristine graphene and reduced graphene oxide.

In Figure 3, we show Kelvin voltage maps of a contacted FGS biased at $V_{ext.}$ = 0 V, +1.0 V, and −1.0 V, respectively. The metal contacts were connected to a source meter, and the left contact was connected to the ground of the KPFM system. At $V_{ext.}$ = 0 V, the KPFM measurement reveals local variations of the material work function. In this case, the Kelvin voltage is given by

$$V_{Kelvin}(x,y) = \frac{1}{e}(\phi_{tip} - \phi_{sample}(x,y)) \qquad (1)$$

where $\phi_{sample}(x,y)$ and ϕ_{tip} are the work functions of the sample and the tip, respectively, and e is the elementary charge. The Kelvin voltage map obtained at zero external bias is shown in Figure 3a. From the data, it is obvious that the Kelvin voltage for both the gold contacts and the FGS (not including wrinkles) is similar, while the Kelvin voltage of the silicon dioxide substrate as compared to the FGS is reduced by about 150 mV indicating a larger work function. According to literature, the work function of gold under ambient conditions was measured with Kelvin probe microscopy to be about 4.7−4.8 eV,[54] whereas a value of about 5.0 eV is found for silicon dioxide.[50] From these data we conclude that the work function of the FGS is about 4.8 ± 0.1 eV.

Thus, our data are in very good agreement with literature values obtained for other types of graphene. For chemically reduced graphene oxide, a work function of 4.88 eV has been previously measured using photoelectron spectroscopy.[64] Kelvin probe force measurements of chemically reduced graphene oxide[65] and mechanically exfoliated graphene[52,65] resulted in values between 4.7 and 5.1 eV. We conclude that our setup works reliably and produces reasonable values for the work function of the involved materials.

The wrinkle-like features on the FGS evident in Figure 3a seem to indicate a local reduction of the Kelvin voltage and thus an increase of the work function on wrinkles compared to the
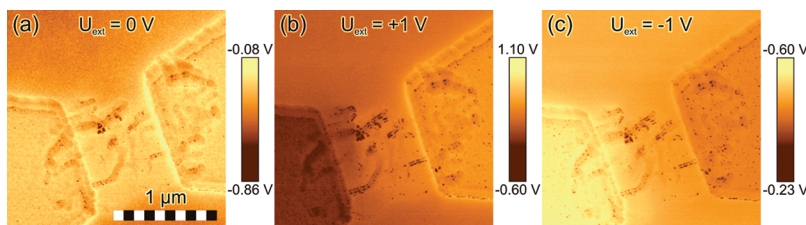
Figure 3. Kelvin voltage maps with external bias (a) 0 V, (b) +1.0 V, and (c) −1.0 V. The left contact was connected to the ground for all the measurements. The voltages represent the work function difference between the AFM tip and the scanned object.

surrounding graphene. However, a Kelvin voltage change is also observed on the Au contacts where graphene wrinkles are covered with metal. A ~100 nm thick Au layer should screen any electrical influence of the graphene underneath, and therefore we have to attribute these features to the abrupt topography changes caused by wrinkles in the FGS instead of a variation of the local work function. This is in agreement with literature data, where it has been suggested that the tip−sample distance, affected by topography at edges of steps and spots, influences the values of the contact potential difference due to averaging effects of the finite tip size.[66,67]

For $V_{ext.} \neq 0$ V, additional information about the sample can be obtained. Upon application of a bias voltage to the gold contacts, an electrical current is flowing through the sample and the Kelvin maps (Figure 3b,c) can be used to determine the potential drop due to dissipative (e.g., Ohmic) losses in the sample during charge transport. Assuming a negligible change of the material work function with external bias, the local voltage drop (as a result of an electrical current flowing through the sheet) can be extracted quantitatively according to[68,69]

$$V_{drop}(x,y) = V_{Kelvin}(V_{ext} \neq 0 \text{ V}) - V_{Kelvin}(V_{ext} = 0 \text{ V})$$

(2)

It is important to note that while the absolute value of the work function is apparently affected by topographic features, the local voltage drop as a result of applied bias ($V_{drop}(x,y)$) is not expected to be significantly influenced by topography.

Since no obvious potential drop between the gold contacts and the FGS can be seen in Figure 3b,c, the contact resistance at the gold−FGS interface must be negligible (which will be discussed in more detail below), and we first analyze the global current−voltage ($I−V$) behavior of the graphene sheet based on applied voltage and measured current. In Figure 4a, we plot the sample current as a function of the total potential drop across the FGS as determined by averaging $V_{drop}(x,y)$ on the gold contact pads and calculating the difference (see histogram in the inset of Figure 4a). For comparison, the current is also plotted as a function of the externally applied bias which includes ohmic losses within the gold contacts and connecting wires. We observe a linear $I−V$ relation which demonstrates the Ohmic character of our FGS within the measured voltage range. From the slope of the $I−V$ curve (triangles) we calculate a resistance of about 2.3 kΩ which corresponds to a sheet resistance and conductivity of ~2.7 kΩ/sq and 3.7×10^5 S/m, respectively, assuming a homogeneous sheet thickness of 1 nm (one single functionalized graphene sheet) and a rectangular sheet geometry of 790 nm × 920 nm (approximated from the actual sheet dimensions (Figure 2a,b). In this calculation, we also assume that the current is uniformly distributed within the sheet. However, our topography
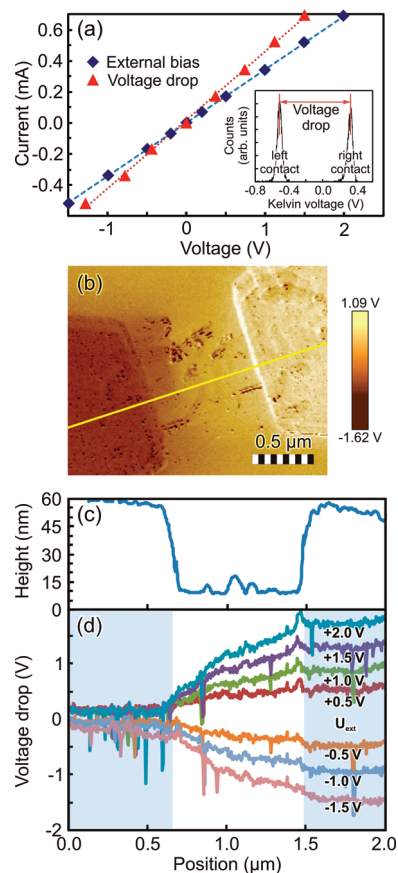

Figure 4. (a) Current versus voltage characteristics of the FGS shown in Figures 2 and 3. For a given current, the blue diamonds indicate the values of the external bias while the red triangles represent data of the voltage drop across the device extracted from KPFM. The inset shows a histogram of the Kelvin data for the left and the right contact, respectively, at $V_{ext} = +1.0$ V. (b) Two-dimensional voltage drop image of the FGS at an external bias of +2 V. (c, d) Line scans of topography and voltage drop with external bias ranging from −1.5 to +2.0 V. The position of the line scan is perpendicular to the metal electrodes (indicated by the yellow line in (b)). The shaded areas in (d) indicate the location of the gold electrodes.

data presented above reveal that the assumption of uniform sheet thickness and therefore homogeneous current and potential distribution does not hold. We therefore need to analyze our data in more detail. While we cannot determine the heterogeneities in the electrical current, we can analyze the spatial distribution of the potential drop across the FGS.

Figure 4b shows $V_{drop}(x,y)$ at +2.0 V bias and a current of 0.68 mA. As mentioned above, we observe no significant potential drop

between the metal contacts and the FGS. This becomes more evident in panels c and d of Figure 4 where we show a profile of the sample topography along the line shown in Figure 4b and the corresponding voltage drop for different applied bias voltages. Considering our measurement accuracy of ~5%, we extract an *upper limit* of the specific contact resistance of $\rho_c = 6.3 \times 10^{-7} \, \Omega \, cm^2$. For this estimation, we assume that due to the good conductivity of the FGSs, the transfer length is equal to the contact length; i.e., the whole contact area of ~0.46 μm^2 contributes to the contact resistance.[70]

Our measured value for the contact resistance is significantly lower than the $10^{-5} \, \Omega \, cm^2$ reported for pure Ni on pristine graphene[44] and lies close to the value of $7.5 \times 10^{-8} \, \Omega \, cm^2$ reported in a recent study for Ti/Au on oxygen plasma treated graphene.[71] There, employing Raman spectroscopy, the authors showed that the decrease of the contact resistance is correlated with an increasing defectiveness of the graphene.[71] This suggests that also for our material the large amount of functional groups and defects and the use of Ti/Au contacts facilitate charge transport between the FGS and the metal electrode. The decreased contact resistance of FGSs compared to pristine graphene may be of importance in applications such as composite materials where contact resistance plays a dominant role. For a firm conclusion, the contact resistance between different graphene sheets needs to be determined in the future.

Figure 4d also shows that the potential does not drop linearly across the sample indicating a locally varying resistance of the FGS. The voltage drop corresponding to a bias voltage of +2 V, for example, exhibits two distinct slopes in the region between the gold contacts. The larger slope between about 0.75 and 1 μm (Figure 4d) has a value of about 2.7 mV/nm and corresponds to a local conductivity of about 3.1×10^5 S/m while the smaller slope between 1 and 1.5 μm indicates a local conductivity of 6.8×10^5 S/m assuming identical local current density and a single layer FGS. The different slopes of the potential may as well be the result of different current densities along the selected line caused by the rather complicated topography of the graphene sheet.

The wrinkles of the FGS which are also evident in Figure 4c have only negligible impact on the measured voltage drop compared to the noise level of the measurement. We tested this last observation further by comparing potential values (V_{drop}) taken on top of a specific wrinkle to values obtained from the direct vicinity (at the same distance to the contacts) of the respective wrinkle (Figure 5a). Apparently, no significant difference between the local potential on and right next to the wrinkles can observed, and we conclude that within our experimental resolution a significant change of the local conductivity at the wrinkles does not occur.

Some of the topographic features visible in panels a and b of Figure 2 most likely are not wrinkles but stacks of several graphene layers. This can be confirmed by the KPFM data, where we found an increase in the conductivity, which agrees with previous measurements on pristine graphene.[53] In Figure 5b, a more detailed line scan of the voltage drop at an external bias of $V_{ext} = +1.0$ V is shown for the specific height step depicted in Figure 2c. The height step results in a pronounced change of the local voltage drop. Similar results are found at different areas of the device. The different slopes of the voltage drop in the region with large (~4.5 nm) and small (~1 nm) heights of 0.44 and 2.7 mV/nm, respectively, correspond to local conductivities (taking into account the measured height as actual
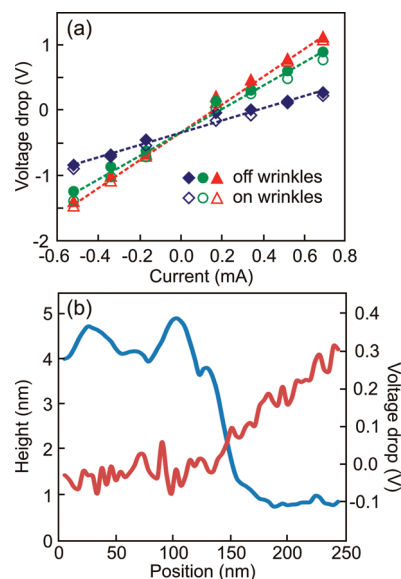

Figure 5. (a) Voltage drop versus current for three selected positions of the device. In each case, data directly on top of a specific wrinkle are compared to data gained from nearby the wrinkles both at the same distance to the contacts. (b) Line scans of topography (blue line) and voltage drop (red line) at the height step indicated by the yellow line in Figure 2a. A drastic change in the voltage drop and thus the local resistivity (given by the slope) is observed for the two different heights.

local thickness of the sample) of 1.9×10^5 and 1.4×10^5 S/m, respectively. For this calculation, we are correcting for the nonperpendicular orientation of the line with respect to the gold contacts and again assume a constant current along the line. We estimate that the resistance of the graphene stack is about 6 times smaller than the resistance of the single layer. Within error, this roughly corresponds to the presumed number of sheets (perhaps four to five) in the FGS stack. On the basis of the observation presented above, we can—due to the complicated sheet topography—only determine the order of magnitude of the conductivity of a one single FGS which we estimate to be 10^5 S/m corresponding to a sheet resistance of about 10 kΩ/sq.

Because the process of fabricating functionalized graphene is a bulk production method which exposes the material of one batch to identical physical conditions, individual sheets should exhibit identical physical properties. In the framework of this study, we conducted successful measurements on two further sheets which were prepared at identical carbon/oxygen ratio. These gave us resistance values close to the one reported above (~1.0 × 10^5 and 0.5 × 10^5 S/m). Because of the limited number of three devices studied, we cannot make firm statements about the scattering of results between different sheets, but we contend that the order of magnitude of the measured conductivities is accurate for the given type of FGSs.

The presence both of a substrate and of adsorbed molecules changes the electrical properties of graphene significantly.[16,59−61,72,73] For example, extrinsic scattering by surface phonons of the substrate limits the room temperature mobility of the charge carriers in graphene,[16] charged impurities on the substrate can cause scattering,[74] and adsorbed molecules result in changes of the charge carrier concentration enabling the use of graphene as a gas sensor.[59,73] It is, therefore, important to consider the impact of the SiO_2 substrate and ambient conditions

on our measurements. The use of a SiO$_2$ substrate may in fact create conditions similar to FGSs in contact with a polymer matrix. It has been shown that graphene in contact with poly-(methyl methacrylate) exhibits the same charge carrier mobility as graphene on silicon dioxide.[75] The prolonged exposure of chemically reduced graphene oxide in a field effect transistor configuration to ambient conditions has been shown to cause a pronounced shift of the gate dependence of the device resistance which is indicative of doping.[55] While we have not yet been able to study the impact of environmental factors on our material, we contend that the measured properties are most likely strongly affected by adsorbed species which may, due to a doping effect, be in parts responsible for the large conductivity we measured. In applications such as polymer composites, however, FGSs are in contact with a variety of chemical species and therefore the study under ambient conditions can be expected to give results which are relevant for real-world applications.

In summary, we have shown that within the applied potential range, FGSs exhibit Ohmic $I-V$ characteristics. Ti/Au contacts are noninvasive as evidenced by the absence of significant potential drops between the metal electrodes and the FGS. We estimate an upper limit of the contact resistivity of 6.3×10^{-7} Ω cm^2. The macroscopic conductivity of the FGS is about 3.7×10^5 S/m which corresponds to a sheet resistance of 2.7 kΩ/sq. Local variations in the measured potential drop across the sheet are probably due to an inhomogeneous current distribution caused by partial stacking of multiple layers of graphene. Wrinkles in the graphene sheet have no significant impact on the local conductivity. Stacking, however, appears to slightly increase the conductivity of the material which has been previously observed for chemically reduced graphene oxide.[55] We have not yet been able to identify a significant influence of the nanometer-sized wrinkling features on the conductivity of the graphene, probably because of the limited spatial resolution of our measurements.

The conductivity of a single FGS is estimated to be on the order of 10^5 S/m which is significantly larger than other reported values for the conductivity of reduced graphene oxide[42,55,56,76] and is only matched by highly defective acid-treated carbon nanosheets.[62] We therefore suggest that the defectiveness of thermally reduced FGSs may in fact contribute to their surprisingly large conductivity. Since their conductivity can be tuned by further thermal reduction and annealing,[77] this renders FGSs a particularly effective additive in composites[26,31,78] requiring scalable production of the material, large intrinsic conductivity, and small contact resistance.

■ AUTHOR INFORMATION

Corresponding Author
*E-mail: wolfgang.mertin@uni-due.de.

Author Contributions
§These authors contributed equally to this work.

■ ACKNOWLEDGMENT

■ REFERENCES

(1) Schafhaeutl, C. J. Prakt. Chem.(Leipzig) **1840**, 21, 570.
(2) Brodie, B. C. Philos. Trans. R. Soc. London **1859**, 149, 249.
(3) Staudenmaier, L. Ber. Dtsch. Chem. Ges. **1898**, 31, 1481–1487.
(4) Boehm, H. P.; Clauss, A.; Fischer, G. O.; Hofmann, U. Z. Anorg. Allg. Chem. **1962**, 316, 119–127.
(5) Boehm, H. P.; Clauss, A.; Hofmann, U.; Fischer, G. O. Z. Naturforsch. **1962**, B 17, 150.
(6) Schniepp, H. C.; Li, J. L.; McAllister, M. J.; Sai, H.; Herrera-Alonso, M.; Adamson, D. H.; Prud'homme, R. K.; Car, R.; Saville, D. A.; Aksay, I. A. J. Phys. Chem. B **2006**, 110, 8535–8539.
(7) McAllister, M. J.; Li, J. L.; Adamson, D. H.; Schniepp, H. C.; Abdala, A. A.; Liu, J.; Herrera-Alonso, M.; Milius, D. L.; Car, R.; Prud'homme, R. K.; Aksay, I. A. Chem. Mater. **2007**, 19, 4396–4404.
(8) Stankovich, S.; Dikin, D. A.; Piner, R. D.; Kohlhaas, K. A.; Kleinhammes, A.; Jia, Y.; Wu, Y.; Nguyen, S. T.; Ruoff, R. S. Carbon **2007**, 45, 1558–1565.
(9) Novoselov, K. S.; Geim, A. K.; Morozov, S. V.; Jiang, D.; Zhang, Y.; Dubonos, S. V.; Grigorieva, I. V.; Firsov, A. A. Science **2004**, 306, 666–669.
(10) Castro Neto, A. H.; Guinea, F.; Peres, N. M. R.; Novoselov, K. S.; Geim, A. K. Rev. Mod. Phys. **2009**, 81, 109–162.
(11) Zhang, Y. B.; Tan, Y. W.; Stormer, H. L.; Kim, P. Nature **2005**, 438, 201–204.
(12) Scarpa, F.; Adhikari, S.; Phani, A. S. Nanotechnology **2009**, 20, 065709.
(13) Lee, C.; Wei, X. D.; Kysar, J. W.; Hone, J. Science **2008**, 321, 385–388.
(14) Balandin, A. A.; Ghosh, S.; Bao, W. Z.; Calizo, I.; Teweldebrhan, D.; Miao, F.; Lau, C. N. Nano Lett. **2008**, 8, 902–907.
(15) Seol, J. H.; Jo, I.; Moore, A. L.; Lindsay, L.; Aitken, Z. H.; Pettes, M. T.; Li, X. S.; Yao, Z.; Huang, R.; Broido, D.; Mingo, N.; Ruoff, R. S.; Shi, L. Science **2010**, 328, 213–216.
(16) Chen, J. H.; Jang, C.; Xiao, S. D.; Ishigami, M.; Fuhrer, M. S. Nat. Nanotechnol. **2008**, 3, 206–209.
(17) Lin, Y. M.; Dimitrakopoulos, C.; Jenkins, K. A.; Farmer, D. B.; Chiu, H. Y.; Grill, A.; Avouris, P. Science **2010**, 327, 662–662.
(18) Geim, A. K.; Novoselov, K. S. Nat. Mater. **2007**, 6, 183–191.
(19) Du, X.; Skachko, I.; Barker, A.; Andrei, E. Y. Nat. Nanotechnol. **2008**, 3, 491–495.
(20) Emtsev, K. V.; Bostwick, A.; Horn, K.; Jobst, J.; Kellogg, G. L.; Ley, L.; McChesney, J. L.; Ohta, T.; Reshanov, S. A.; Rohrl, J.; Rotenberg, E.; Schmid, A. K.; Waldmann, D.; Weber, H. B.; Seyller, T. Nat. Mater. **2009**, 8, 203–207.
(21) Krupka, J.; Strupinski, W. Appl. Phys. Lett. **2010**, 96, 3.
(22) Li, X. S.; Cai, W. W.; An, J. H.; Kim, S.; Nah, J.; Yang, D. X.; Piner, R.; Velamakanni, A.; Jung, I.; Tutuc, E.; Banerjee, S. K.; Colombo, L.; Ruoff, R. S. Science **2009**, 324, 1312–1314.
(23) Reina, A.; Jia, X. T.; Ho, J.; Nezich, D.; Son, H. B.; Bulovic, V.; Dresselhaus, M. S.; Kong, J. Nano Lett. **2009**, 9, 30–35.
(24) Stoller, M. D.; Park, S. J.; Zhu, Y. W.; An, J. H.; Ruoff, R. S. Nano Lett. **2008**, 8, 3498–3502.
(25) Paek, S. M.; Yoo, E.; Honma, I. Nano Lett. **2009**, 9, 72–75.
(26) Wang, D. H.; Choi, D. W.; Li, J.; Yang, Z. G.; Nie, Z. M.; Kou, R.; Hu, D. H.; Wang, C. M.; Saraf, L. V.; Zhang, J. G.; Aksay, I. A.; Liu, J. ACS Nano **2009**, 3, 907–914.
(27) Yoo, E.; Kim, J.; Hosono, E.; Zhou, H.; Kudo, T.; Honma, I. Nano Lett. **2008**, 8, 2277–2282.
(28) Pumera, M.; Ambrosi, A.; Bonanni, A.; Chng, E. L. K.; Poh, H. L. TRAC, Trends Anal. Chem. **2010**, 29, 954–965.
(29) Punckt, C.; Pope, M. A.; Liu, J.; Lin, Y. H.; Aksay, I. A. Electroanalysis **2010**, 22, 2834–2841.
(30) Shao, Y. Y.; Wang, J.; Wu, H.; Liu, J.; Aksay, I. A.; Lin, Y. H. Electroanalysis **2010**, 22, 1027–1036.
(31) Ramanathan, T.; Abdala, A. A.; Stankovich, S.; Dikin, D. A.; Herrera-Alonso, M.; Piner, R. D.; Adamson, D. H.; Schniepp, H. C.; Chen, X.; Ruoff, R. S.; Nguyen, S. T.; Aksay, I. A.; Prud'homme, R. K.; Brinson, L. C. Nat. Nanotechnol. **2008**, 3, 327–331.

F

dx.doi.org/10.1021/nl201070c |Nano Lett. XXXX, XXX, 000–000

(32) Stankovich, S.; Dikin, D. A.; Dommett, G. H. B.; Kohlhaas, K. M.; Zimney, E. J.; Stach, E. A.; Piner, R. D.; Nguyen, S. T.; Ruoff, R. S. *Nature* **2006**, *442*, 282–286.

(33) Zhu, Y. W.; Murali, S.; Cai, W. W.; Li, X. S.; Suk, J. W.; Potts, J. R.; Ruoff, R. S. *Adv. Mater.* **2010**, *22*, 3906–3924.

(34) Hummers, W. S.; Offeman, R. E. *J. Am. Chem. Soc.* **1958**, *80*, 1339–1339.

(35) Wen, X.; Garland, C. W.; Hwa, T.; Kardar, M.; Kokufuta, E.; Li, Y.; Orkisz, M.; Tanaka, T. *Nature* **1992**, *355*, 426–428.

(36) Segal, M. *Nat. Nanotechnol.* **2009**, *4*, 611–613.

(37) Langley, L. A.; Villanueva, D. E.; Fairbrother, D. H. *Chem. Mater.* **2006**, *18*, 169–178.

(38) Kudin, K. N.; Ozbas, B.; Schniepp, H. C.; Prud'homme, R. K.; Aksay, I. A.; Car, R. *Nano Lett.* **2008**, *8*, 36–41.

(39) Gomez-Navarro, C.; Meyer, J. C.; Sundaram, R. S.; Chuvilin, A.; Kurasch, S.; Burghard, M.; Kern, K.; Kaiser, U. *Nano Lett.* **2010**, *10*, 1144–1148.

(40) Bagri, A.; Mattevi, C.; Acik, M.; Chabal, Y. J.; Chhowalla, M.; Shenoy, V. B. *Nat. Chem.* **2010**, *2*, 581–587.

(41) Roy-Mayhew, J. D.; Bozym, D. J.; Punckt, C.; Aksay, I. A. *ACS Nano* **2010**, *4*, 6203–6211.

(42) Jung, I.; Dikin, D. A.; Piner, R. D.; Ruoff, R. S. *Nano Lett.* **2008**, *8*, 4283–4287.

(43) Huard, B.; Stander, N.; Sulpizio, J. A.; Goldhaber-Gordon, D. *Phys. Rev. B* **2008**, *78*, 121402.

(44) Venugopal, A.; Colombo, L.; Vogel, E. M. *Appl. Phys. Lett.* **2010**, *96*, 013512.

(45) Deshpande, A.; Bao, W.; Zhao, Z.; Lau, C. N.; LeRoy, B. J. *Phys. Rev. B* **2011**, *83*, 155409.

(46) Xu, K.; Cao, P. G.; Heath, J. R. *Nano Lett.* **2009**, *9*, 4446–4451.

(47) de Parga, A. L. V.; Calleja, F.; Borca, B.; Passeggi, M. C. G.; Hinarejos, J. J.; Guinea, F.; Miranda, R. *Phys. Rev. Lett.* **2008**, *100*, 056807.

(48) Nonnenmacher, M.; Oboyle, M. P.; Wickramasinghe, H. K. *Appl. Phys. Lett.* **1991**, *58*, 2921–2923.

(49) Girard, P. *Nanotechnology* **2001**, *12*, 485–490.

(50) Vinaji, S.; Lochthofen, A.; Mertin, W.; Regolin, I.; Gutsche, C.; Prost, W.; Tegude, F. J.; Bacher, G. *Nanotechnology* **2009**, *20*, 385702.

(51) Datta, S. S.; Strachan, D. R.; Mele, E. J.; Johnson, A. T. C. *Nano Lett.* **2009**, *9*, 7–11.

(52) Lee, N. J.; Yoo, J. W.; Choi, Y. J.; Kang, C. J.; Jeon, D. Y.; Kim, D. C.; Seo, S.; Chung, H. J. *Appl. Phys. Lett.* **2009**, *95*, 222107.

(53) Yu, Y. J.; Zhao, Y.; Ryu, S.; Brus, L. E.; Kim, K. S.; Kim, P. *Nano Lett.* **2009**, *9*, 3430–3434.

(54) Filleter, T.; Emtsev, K. V.; Seyller, T.; Bennewitz, R. *Appl. Phys. Lett.* **2008**, *93*, 133117.

(55) Gomez-Navarro, C.; Weitz, R. T.; Bittner, A. M.; Scolari, M.; Mews, A.; Burghard, M.; Kern, K. *Nano Lett.* **2007**, *7*, 3499–3503.

(56) Sundaram, R. S.; Gomez-Navarro, C.; Lee, E. J. H.; Burghard, M.; Kern, K. *Appl. Phys. Lett.* **2009**, *95*, 223507.

(57) Novoselov, K. S.; Geim, A. K.; Morozov, S. V.; Jiang, D.; Katsnelson, M. I.; Grigorieva, I. V.; Dubonos, S. V.; Firsov, A. A. *Nature* **2005**, *438*, 197–200.

(58) Novoselov, K. S.; Jiang, D.; Schedin, F.; Booth, T. J.; Khotkevich, V. V.; Morozov, S. V.; Geim, A. K. *Proc. Natl. Acad. Sci. U.S.A.* **2005**, *102*, 10451–10453.

(59) Schedin, F.; Geim, A. K.; Morozov, S. V.; Hill, E. W.; Blake, P.; Katsnelson, M. I.; Novoselov, K. S. *Nat. Mater.* **2007**, *6*, 652–655.

(60) Bolotin, K. I.; Sikes, K. J.; Jiang, Z.; Klima, M.; Fudenberg, G.; Hone, J.; Kim, P.; Stormer, H. L. *Solid State Commun.* **2008**, *146*, 351–355.

(61) Chen, J. H.; Cullen, W. G.; Jang, C.; Fuhrer, M. S.; Williams, E. D. *Phys. Rev. Lett.* **2009**, *102*, 236805.

(62) Jafri, S. H. M.; Carva, K.; Widenkvist, E.; Blom, T.; Sanyal, B.; Fransson, J.; Eriksson, O.; Jansson, U.; Grennberg, H.; Karis, O.; Quinlan, R. A.; Holloway, B. C.; Leifer, K. *J. Phys. D* **2010**, *43*, 045404.

(63) Schniepp, H. C.; Kudin, K. N.; Li, J. L.; Prud'homme, R. K.; Car, R.; Saville, D. A.; Aksay, I. A. *ACS Nano* **2008**, *2*, 2577–2584.

(64) Kong, B. S.; Geng, J. X.; Jung, H. T. *Chem. Commun.* **2009** 2174–2176.

(65) Yin, Z. Y.; Wu, S. X.; Zhou, X. Z.; Huang, X.; Zhang, Q. C.; Boey, F.; Zhang, H. *Small* **2010**, *6*, 307–312.

(66) Jacobs, H. O.; Leuchtmann, P.; Homan, O. J.; Stemmer, A. *J. Appl. Phys.* **1998**, *84*, 1168–1173.

(67) Sadewasser, S.; Leendertz, C.; Streicher, F.; Lux-Steiner, M. C. *Nanotechnology* **2009**, *20*, 505503.

(68) Katzer, K. D.; Mertin, W.; Bacher, G.; Jaeger, A.; Streubel, K. *Appl. Phys. Lett.* **2006**, *89*, 103522.

(69) Leveque, G.; Girard, P.; Skouri, E.; Yarekha, D. *Appl. Surf. Sci.* **2000**, *157*, 251–255.

(70) Grosse, K. L.; Bae, M. H.; Lian, F. F.; Pop, E.; King, W. P. *Nat. Nanotechnol.* **2011**, *6*, 287–290.

(71) Robinson, J. A.; LaBella, M.; Zhu, M.; Hollander, M.; Kasarda, R.; Hughes, Z.; Trumbull, K.; Cavalero, R.; Snyder, D. *Appl. Phys. Lett.* **2011**, *98*, 3.

(72) Castro, E. V.; Ochoa, H.; Katsnelson, M. I.; Gorbachev, R. V.; Elias, D. C.; Novoselov, K. S.; Geim, A. K.; Guinea, F. *Phys. Rev. Lett.* **2010**, *105*, 4.

(73) Lu, G. H.; Ocola, L. E.; Chen, J. H. *Appl. Phys. Lett.* **2009**, *94* 083111.

(74) Chen, J. H.; Jang, C.; Adam, S.; Fuhrer, M. S.; Williams, E. D.; Ishigami, M. *Nat. Phys.* **2008**, *4*, 377–381.

(75) Morozov, S. V.; Novoselov, K. S.; Katsnelson, M. I.; Schedin, F.; Elias, D. C.; Jaszczak, J. A.; Geim, A. K. *Phys. Rev. Lett.* **2008**, *100*, 4.

(76) Li, X. L.; Zhang, G. Y.; Bai, X. D.; Sun, X. M.; Wang, X. R.; Wang, E.; Dai, H. J. *Nat. Nanotechnol.* **2008**, *3*, 538–542.

(77) Korkut, S.; Ozbas, B.; Milius, D. L.; Liu, J.; Aksay, I. A. Submitted, 2011.

(78) Wang, D. H.; Kou, R.; Choi, D.; Yang, Z. G.; Nie, Z. M.; Li, J.; Saraf, L. V.; Hu, D. H.; Zhang, J. G.; Graff, G. L.; Liu, J.; Pope, M. A.; Aksay, I. A. *ACS Nano* **2010**, *4*, 1587–1595.